The Enhanced Self-Lift Luo Converter with Qhbm for Maximum Power Extraction on PV Charging Station

Aripriharta [1], Fiqi Ardian Pratama Sudarto [2], Irham Fadlika [3], Sujito [4], Muhammad Cahyo Bagaskoro [5], Saodah Omar [6], Norsanah Binti Rosmin [7]

[1] Centre of Advance Material of Renewable energy, Universitas Negeri Malang, Indonesia
[2,3,4,5] Department of Electrical Engineering and Informatics, Universitas Negeri Malang, Indonesia
[6] School of Electrical Engineering, College of Engineering, University Technology MARA, Malaysia
[7] Centre of Electrical Energy System (CEES), Universiti Teknologi Malaysia, Sekolah Kejuruteraan Elektrik, Fakulti Kejuruteraan, Malaysia
Corresponding: aripriharta.ft@um.ac.id

Abstract

This journal presents the development of an innovative algorithm for Maximum Power Point Tracking (MPPT) utilizing the Enhanced Self Lift Luo Converter (ESLLC) developed through Queen Honey Bee Migration (QHBM). The QHBM used for MPPT employs a queen-based decision-making approach to determine the optimal point on solar panels. The queen continuously searches for the Maximum Power Point (MPP), and upon locating it, ceases tracking and starts building a nest. Once the nest is established, the queen resumes the search for MPP. The testing simulation evaluates computing speed, durability, and MPP's margin errors. MATLAB/Simulink is employed for verification. The simulation results demonstrate that the QHBM surpasses other algorithms like PSO, P&O, and FLC in terms of computing speed, durability, and MPP margin errors. The QHBM-based MPPT exhibits superior responsiveness to changes in irradiation and temperature compared to alternative algorithms. This proposed algorithm effectively adapts to varying environmental conditions that influence irradiation and temperature changes. Consequently, the suggested algorithm holds significant promise for practical implementation in dynamic environmental settings.

Keywords

Enhanced Self Lift Luo Converter, MPPT, QHBM

INTRODUCTION

Renewable Energy Sources (RES) emerge as the most favorable option amid declining conventional resource reserves (fossil fuels) and escalating environmental pollution levels (Blaabjerg, 2016). Global initiatives are evident, focusing on expediting the adoption of RES, particularly solar panels (Elboid, 2015). However, solar panels (PV) do exhibit limitations, such as relatively low PV conversion efficiency, which typically ranges from 8% to 25% (Green, 2018). Moreover, the power generated by solar panels is non-linear concerning external conditions, including variations in solar irradiation, surface temperature of solar panels, and the presence of shadows.

The non-linear nature of power generated by solar panels necessitates adaptive control for optimal performance (Enrique, 2010). Currently, the most effective technique for this purpose is maximum power point tracking (MPPT), which aims to ensure that the PV system consistently operates at its maximum power point (MPP) (Kandemir, 2019). Over time, MPPT techniques have evolved significantly, transitioning from simple to complex implementations utilizing soft computing. The simplest MPPT techniques typically predict MPP based on the gain of the short circuit current or open circuit voltage. However, these techniques prove unreliable when there are variations in irradiation levels.

Hill climbing MPPTs, such as Perturb & Observe (P&O) and Incremental Conductance (IC), exhibit superior accuracy compared to Fuzzy Logic Control (FLC) and Fractional Short-Circuit (FSC) methods. P&O, known for its simplicity and cost-effectiveness, finds widespread use in commercial MPPTs (Titri, 2017). Nevertheless, both P&O and IC suffer from extended convergence times and oscillations around the MPP, particularly when confronted with changes in irradiation levels. To address the limitations of traditional MPPT techniques, researchers have explored hybrid MPPT approaches, which combine traditional methods with soft computing to handle non-linear and uncertain conditions effectively. Fuzzy Logic Control (FLC) and Particle Swarm Optimization (PSO) have emerged as two commonly utilized techniques for this purpose (Sundareswaran, 2015). While FLC can offer optimal results, it demands complex computations, whereas PSO requires considerable time to complete the computations. All computational techniques derived from the MPPT algorithm require implementation in the dc-dc converter to ensure optimal operation of the PV output, adhering to maximum power point tracking (MPP) principles (Bendip, 2015). Research by Islam (2018) highlights that each dc-dc converter comes with its specific limitations, making the selection and design process crucial for the overall system. Previous studies have successfully employed a choke converter for

MPP, as it proves well-suited to handle variations in environmental conditions and loads. In this research, the focus is on utilizing the luo converter, recognized for its ability to elevate low input voltage values to higher output voltage levels (Kamat, 2018). Combining the self-lift technique with the MPPT controller has resulted in effective tracking of the required output voltage (Amirtharja, 2017). This study explores the application of a novel MPPT algorithm technique, namely MPPT based on Queen Honey Bee Migration (QHBM). The QHBM technique has shown promising results in various applications, boasting faster computational algorithms compared to other methods (Jong, 2017).

This research focuses on exploring the application of the MPPT technique based on Queen Honey Bee Migration (QHBM) to effectively tackle the challenges posed by dynamic environmental conditions in real-time. The study utilizes resistive loads to evaluate the algorithm's performance when dealing with DC housing loads, while capacitive loads are employed to simulate real-life battery usage for electrical energy storage. To match the required capacitive load value, the research employs the Luo Enhanced Self Lift Converter, which acts as a voltage regulator. The entire investigation is simulated using Matlab/Simulink, enabling accurate and comprehensive analysis of the proposed MPPT algorithm's capabilities.

MATERIAL METHODS

1. Enhanced Self-Lift Luo Converter

The working principle of the Enhanced Self Lift Luo Converter (ESLLC) involves two distinct modes: mode 1 and mode 2. In mode 1, when the MOSFET is closed, the diode D1 becomes conductive. During this phase, inductor L1 accumulates energy from the source voltage and charges the capacitor C. Since the impedance at capacitor C is zero, a continuous charging process occurs, maintaining the conduction of diode D1. In mode 2, current iL1 flows through diode D, charging capacitor C and subsequently feeding current into capacitor C1 to increase the current in iL2. Inductor L1 transfers the stored energy to capacitor C1 and the load through Inductor 2. The duty ratio (D) is determined using the following equation 1 and figure 1.

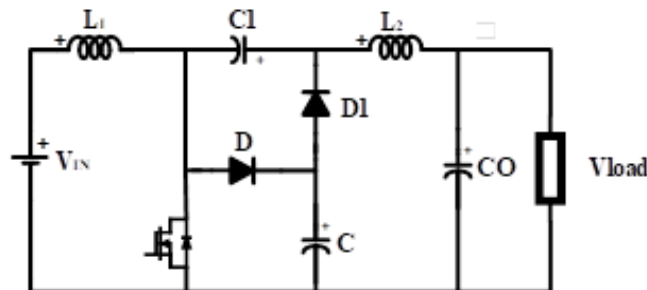$$V_{out} = \frac{(2 - D)}{(1 - D)} V_{in}$$

(1)

Figure 1. Enhanced Self Lift Luo Converter

2. Solar Panel

According to research conducted by Femia (2012), solar panels, or photovoltaic (PV) panels, consist of a large number of solar cells arranged in both series and parallel configurations. These configurations play an important role in determining the voltage and current levels generated by the solar panels. When solar cells are connected in series to form a string, it impacts the total PV voltage, and the number of solar cells arranged in parallel configurations impacts the PV current level.
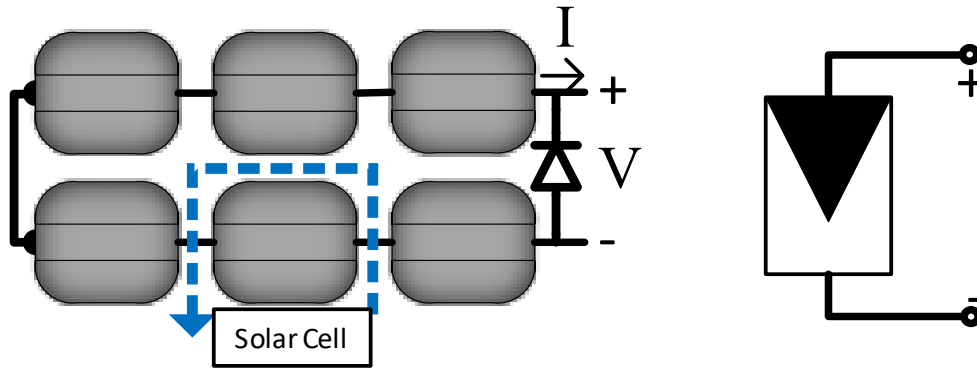
Figure 2. PV Characteristic

A. PV Characteristics

The performance of PV systems is intricately linked to prevailing environmental conditions, with solar irradiation and temperature playing pivotal roles in shaping PV output. Notably, Figure 3 illustrates the profound impact of temperature on PV voltage output, as evidenced by the dynamic fluctuations in voltage values corresponding to varying ambient temperatures. Conversely, Figure 4 demonstrates the correlation between PV current and solar radiation variations, elucidating how changes in solar radiation levels lead to corresponding shifts in PV current output.
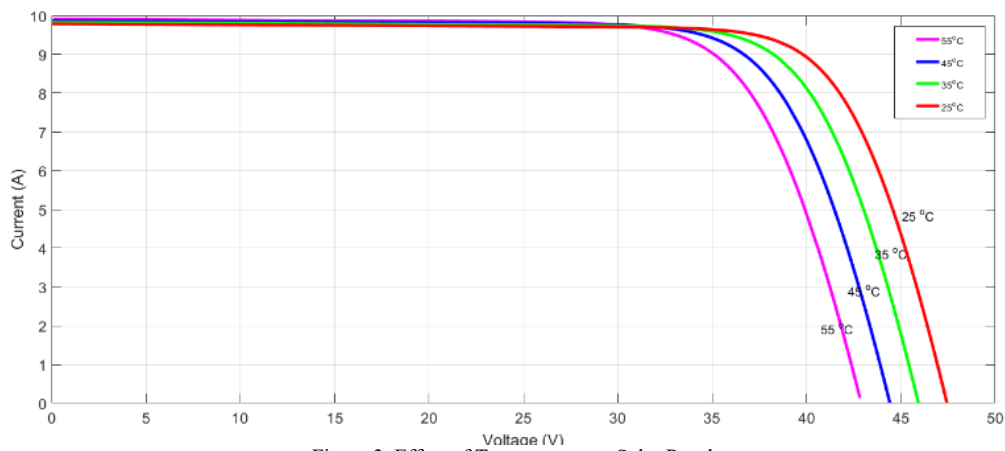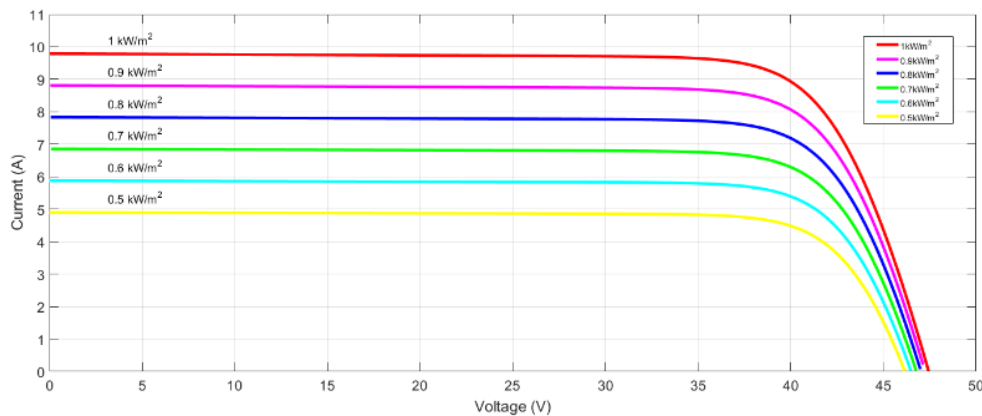

Figure 3. Effect of Temperature on Solar Panels

Figure 4. Radiation Effect on Solar Panels

The temperature change in Figure 2.2 is slow enough that the temperature value is often assumed to be constant. This assumption was also carried out in this study. In addition, the voltage is independent of irradiation. On the other hand, PV current is also affected by temperature. The statement is by Equation 1.

$$I_{ph} = I_{ph,STC} \frac{G}{G_{STC}} [1+\alpha_1(T-T_{STC})] \tag{2}$$

$$T = T_a + \frac{NOCT - 20}{800} . G \tag{3}$$

Figure 5 vividly presents the distinct characteristics of a PV system. Within this graph, three pivotal points stand out: short circuit (SC) conditions, open circuit (OC) conditions, and maximum power conditions (MP). The short circuit state emerges when the voltage reaches zero while the short circuit current (ISC) prevails. Correspondingly, the open circuit state arises as the current reaches zero, accompanied by the open voltage value (VOC). Consequently, both these scenarios yield a power output of zero. Notably, the PV system's optimal power generation, denoted by the production of maximum power, is signified by the intersection of maximum voltage (VMP) and maximum current (IMP) values.
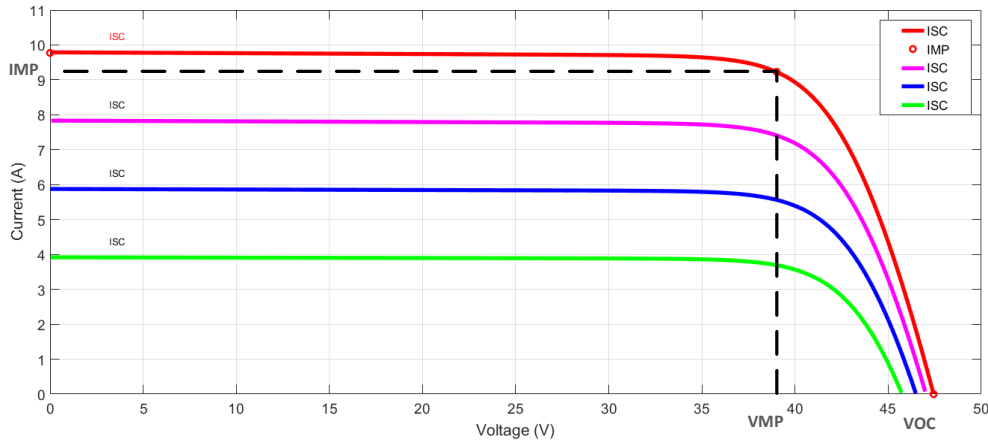

Figure 5. Solar Panel Characteristic Graph

B. Solar Cell Equivalent Circuit

The PV equivalent circuit model serves as a valuable tool for dissecting PV behavior and deriving its mathematical representation. The essential parameters can be acquired via data garnered from meticulous experimental measurements or extracted from available datasheets. Illustrated in Figure 6, the ensuing sections detail the equivalent circuitry of solar cells, along with the computation of power losses attributed to the two resistors within the PV system.
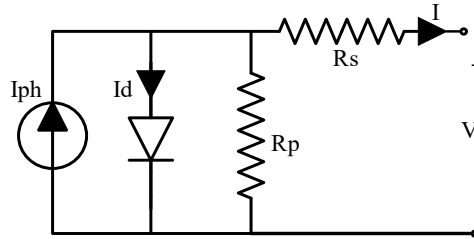

Figure 6. Solar Panels Equivalent Circuit

To obtain the value of the current issued by PV can use equation 3 by using Kirchhoff's law:

$$I = I_{PH} - I_{SAT} . \left(e^{\frac{V+I.R_S}{\eta V_t}} - 1 \right) - \frac{V + I.R_S}{R_p} \tag{4}$$

Equation 3 encapsulates the PV current denoted as "I," wherein ISAT represents the saturation current at the PN Junction as determined by Equation 5. The parameter "n" stands for the ideal factor, while "Rs" signifies the series resistor and "Rp" represents the parallel resistor. Additionally, "Vt" corresponds to the thermal voltage computed using Equation 6. Establishing the temperature is the purpose of Equation 7, paving the way for Equations 8 and 9, both of which constitute the power equations serving as the foundation for the fitness function.

$$I_{SAT} = C.T^3.e^{\left(\frac{E_{gap}}{k.T}\right)} \tag{6}$$

$$T = \frac{V_{oc} - V_{ocr}}{K_v} - T_r \tag{7}$$

$$V = V_T Ln\left[\left(1 - \frac{I}{I_{sc}}\right)\left(exp\left(\frac{V_{oc}}{V_T}\right) - 1\right) + 1\right] - R_s I \tag{8}$$

$$P = \left(V_T Ln\left[\left(1 - \frac{I}{I_{sc}}\right)\left(exp\left(\frac{V_{oc}}{V_T}\right) - 1\right) + 1\right] - R_s I\right).I \tag{9}$$

"C" embodies the temperature coefficient, while "Egap" symbolizes the band gap of the semiconductor material—given as Egap = 1.8x10-19J for crystalline silicon. The value of "k" stands at 1.3806503x10-23 J/K, representing the renowned Boltzmann constant, while "q" quantifying the charge of an electron, is expressed as q = 1.60217646x10-19 C.

3. Solar Queen Honey Bee Migration

Within the QHBM algorithm (Jong 2017), a striking analogy unfolds, with the queen donning the role of a decisive authority and the bee soldiers serving as able guides. The queen orchestrates her migration to fresh domains by relying upon the sector adorned with the utmost energy, dutifully monitored by her loyal bee soldiers. Figure 7 visually encapsulates this process. This transition prompts the division of the Sector into 8 sub-regions, each aligning with the cardinal directions. Broadly speaking, the QHBM algorithm comprises three distinct phases: initial conditions, sector probabilities, and journeys. The following elucidates the intricacies of these stages :

a. Initialize conditions. The Queen's initial position (Vpv, Ppv), Queen bee Distance to destination (RQHBM), and Queen's Resistance to disturbance (Gs) have been defined.

b. Calculation of sector probabilities. After getting the Initialization Condition, the Bee Soldier spreads out to some 8 sectors. Each bee warrior (cj) has a joy value. Next, calculate the probability value (pk) entering each Within a given sector, the stimulus value is encapsulated by Equation (10), whereas Equation (11) delineates the probability value as follows : Where "j" stands for the unique identity of the bee soldier, "k" signifies the sector's identity, "n" represents the count of scout bees, and "er(ij)" captures the residual energy of the particular bee soldier.

Guiding the Honeybee Queen's journey, a pivotal aspect of the process involves her relocation to the sector boasting the most elevated score. This shift, however, isn't exempt from the influence of disturbance, with the radius value explicitly defined in Equation (12). Subsequently, Equation (13) plays a role in establishing the Vpv value, followed by Equation (14) which contributes to the calculation of Ppv. As the Queen embarks on successive journeys, the equation (15) comes into play, encapsulating her fortitude against interference.

$$C_j = \frac{1}{n}\sum_{j=1}^{n} e_{r(ij)} \tag{10}$$

$$P_k = \frac{C_j}{\sum_{j=1}^{8} C_j} \tag{11}$$

$$r_m^{(ith+1)} = (1 - G_s^{(ith)} \tag{12}$$

$$V_{pv}^{(ith+1)} = V_{pv}^{(ith+1)} + r_m^{(ith+1)}.cos\theta^{(ith+1)} \tag{13}$$

$$P_{pv}^{(ith+1)} = P_{pv}^{(ith+1)} + r_m^{(ith+1)}.sin\theta^{(ith+1)} \tag{14}$$

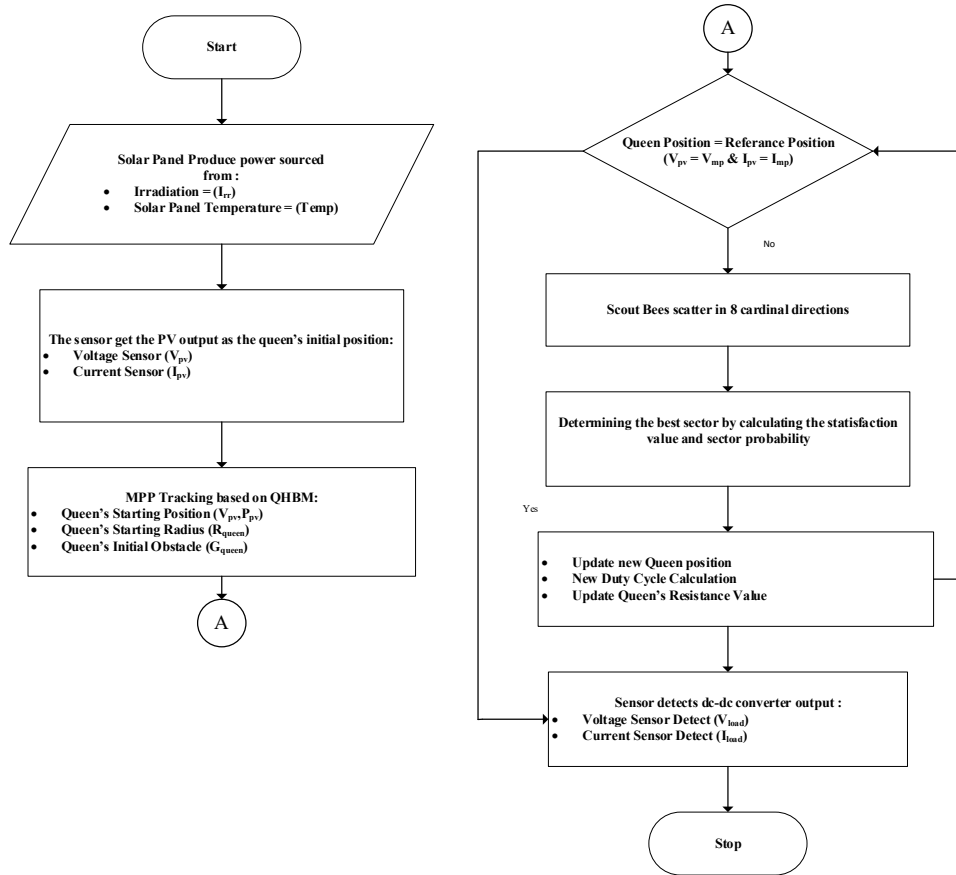$$G_s^{(ith+1)} = G_m^{(ith+1)}.rand \tag{15}$$

Figure 7. QHBM-based MPPT

A. System Block Diagram

Presented in Figure 8, the system's block diagram serves as a visual representation of the framework studied. Central to this arrangement is a photovoltaic (PV) source tasked with supplying the load. In response to shifting environmental conditions, the power output of the PV source exhibits variations. To tackle this challenge, the study harnesses the QHBM algorithm, meticulously shaping the PV power output towards its zenith. This fine-tuning entails the manipulation of duty cycles, a process driven by the QHBM algorithm using core parameters Vpv and Ppv. These critical figures are derived from voltage and current sensors. While Vpv originates from the voltage sensor, Ppv emerges from the product of Vpv and Ipv. The algorithm operates relentlessly until Vpv and Ppv converge with the reference values (Vmp and Pmax). Upon reaching this pivotal reference point, the algorithm halts its iterations. As a further safeguard, measurements of Vload and Iload are employed, guaranteeing that the load receives power conforming to the prescribed specifications.
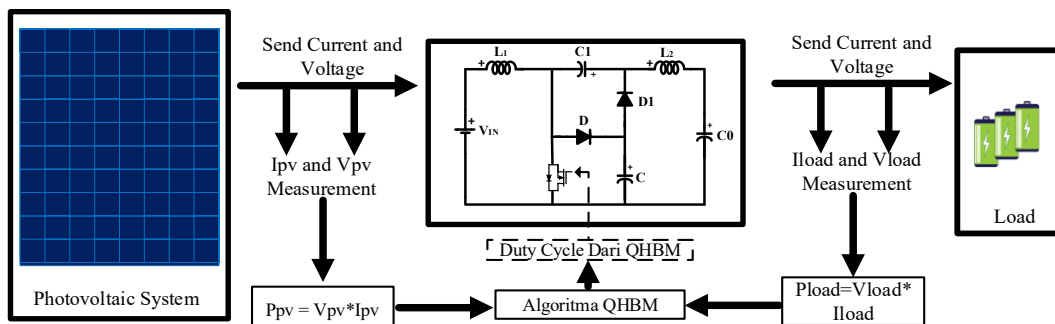

Figure 8. System Block Diagram

B. PV

In this study using the NSP D6M360E4 solar panel, as presented in Table 1 as follows:

TABLE 1

PV SPECIFICATIONS

Parameter	NSP D6M360E4A
Pmax	360 W
Voc	47.44 V
Vmp	39.01 V
Imp	9.23 A
Isc	9.77 A
Voc	47.44 V

Figures 9 and 10 showcase the characteristic P-V and I-V curves. These curves hold the key to identifying the maximum power point, a value intricately tied to the incident radiation. Upon scrutinizing the curves, a distinct pattern emerges: with 1000 W/m2 radiation, the power intake peaks at 360 Watts; conversely, when the radiation plummets, the minimal power acquired bottoms out at 230 Watts.
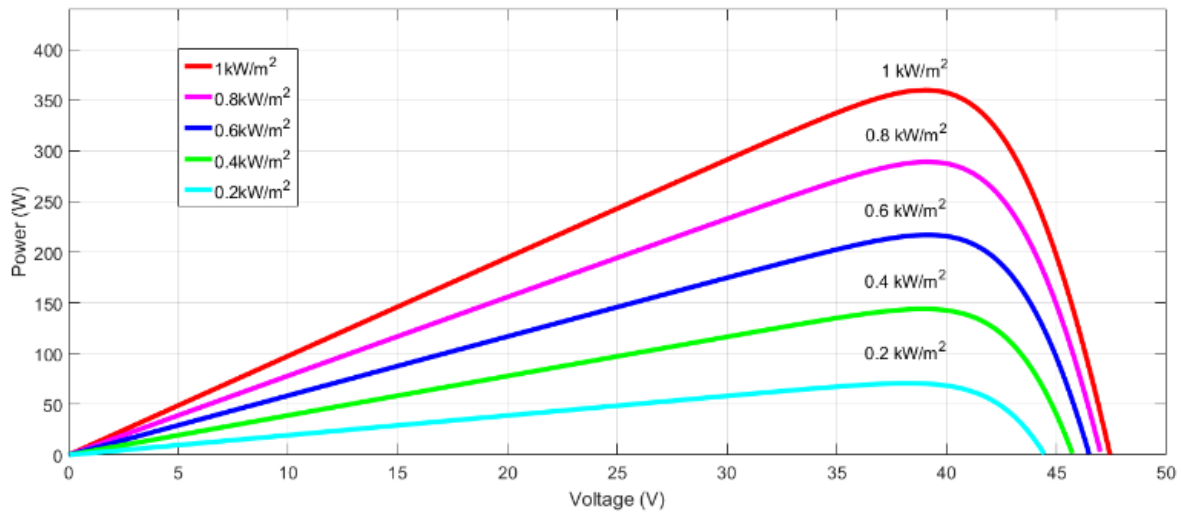

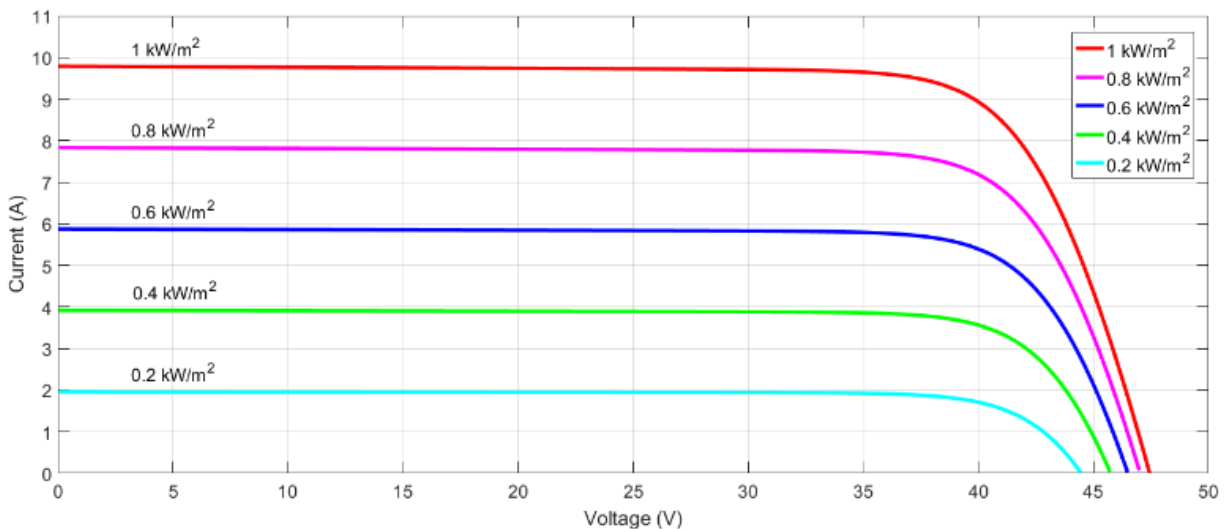Figure 9. P-V NSP D6M360E4 Characteristic Curve

Figure 10. C-V NSP D6M360E4 Characteristic Curve

C. QHBM Performance Analysis facing Environmental Changes in Real-Time

In this study uses, alterations in environmental conditions were directly gauged using a Solar Power Meter, ensuring precision in data acquisition. The collection window spanned from 08:00 AM to 3:00 PM, capturing a substantial portion of the daylight hours. This study adopted a strategic approach, concentrating on temperature fluctuations, thereby assuming a constant temperature for the PV while allowing solar radiation to fluctuate naturally. Evaluating the performance of the QHBM-based MPPT method entailed a comprehensive juxtaposition against three comparison algorithms: PSO, P&O, and FLC. The crux of the comparison rested on the duration each algorithm required to yield the maximal power output. Captured concisely in Table 2, the ever-changing environmental conditions are succinctly presented for reference.

TABLE 2

SOLAR RADIATION CHANGE DATA

Solar Radiation (W/m²)	Temperature (Celcius)
762.8	25
926.1	25
762.7	25
316.3	25
1053.2	25
304.7	25
208.3	25
935.7	25
158.8	25
257,5	25
240	25
116	25
170,3	25
233.2	25
182.3	25
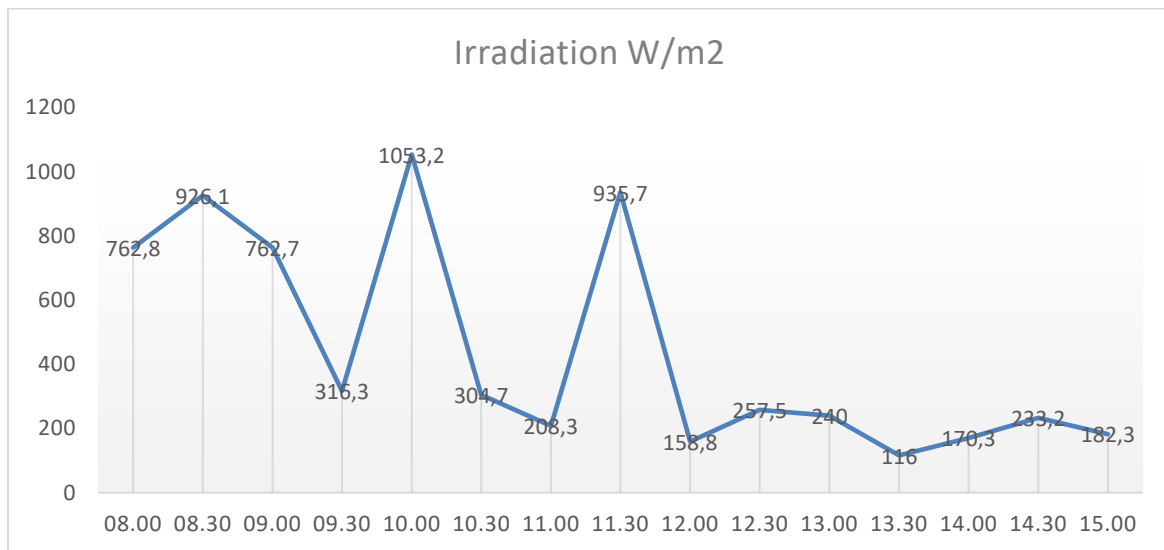
Figure 11. Radiation Testing Parameters

Figure 11, derived from real-time irradiation data acquired through a solar power meter, provides a visual representation of the parameter range under scrutiny in this study, spanning from the minimum to the maximum irradiation levels. To comprehensively evaluate these parameters, simulation was executed employing the Matlab/Simulink software. The ensuing outcomes of this simulation endeavor are elucidated below. Figure 12 and 13 shows the irradiation test parameters, and the connection to the current from the irradiation changes in real time.

Figure 12. P-V Testing Parameters

Figure 13. C-V Testing Parameters
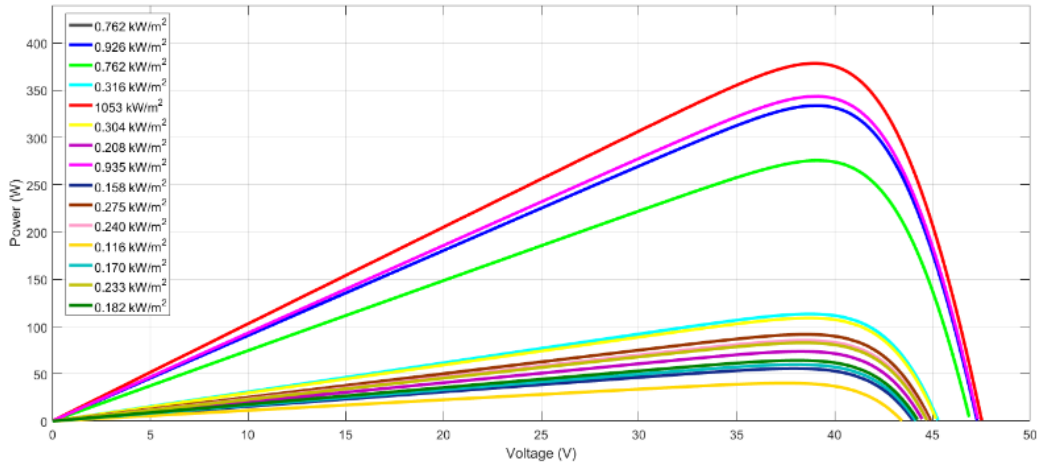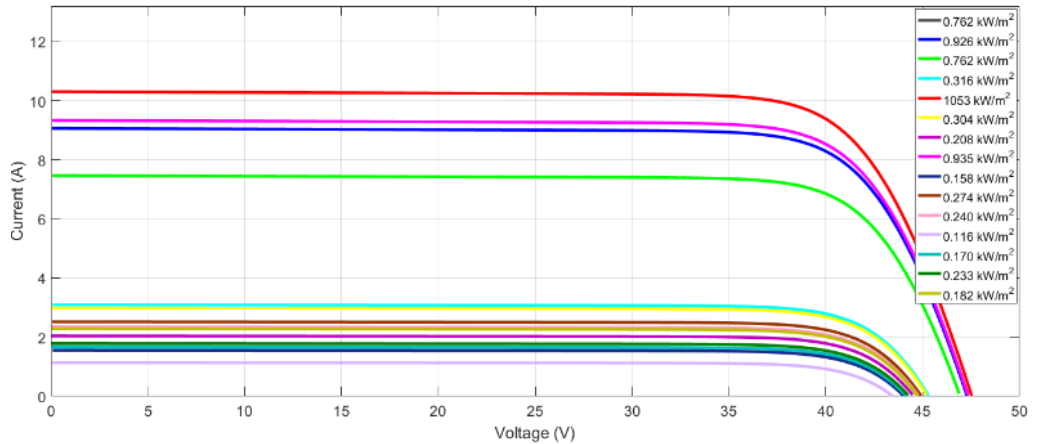
D. QHBM Parameter Parameter Testing Simulation Results

Table 3 highlights the simulation outcomes for both the most optimal and least favorable QHBM parameter configurations. The parameters scrutinized encompass the maximum iterations of the queen bee's journey, the radius of the queen bee's influence, and the quantity of bee soldiers, all subjected to the identical environmental conditions of solar irradiation and temperature.

TABLE 3

QHBM PARAMETER TESTING SIMULATION RESULT

No	Scout Bee	Radius	Iterasi	Vin (Volt)	Vmp (Volt)	Vqueen (Volt)	Pin (Watt)	Pmp (Watt)	Pqueen (Watt)
1	18	5	100	39.2	38.96	38.2	367.65	378.5	377.7
2	18	10	100	39.2	38.96	39	367.65	378.5	375
3	24	10	100	39.2	38.96	39.4	367.65	378.5	376.5
4	24	5	100	39.2	38.96	38.5	367.65	378.5	373.3
5	24	5	50	39.2	38.96	38.6	367.65	378.5	368.8
6	18	10	50	39.2	38.96	36.5	367.65	378.5	376.9
7	24	10	50	39.2	38.96	38.4	367.65	378.5	374.4
8	18	5	50	39.2	38.96	38.1	367.65	378.5	376.4

*The best QHBM-Based MPPT Simulation Results
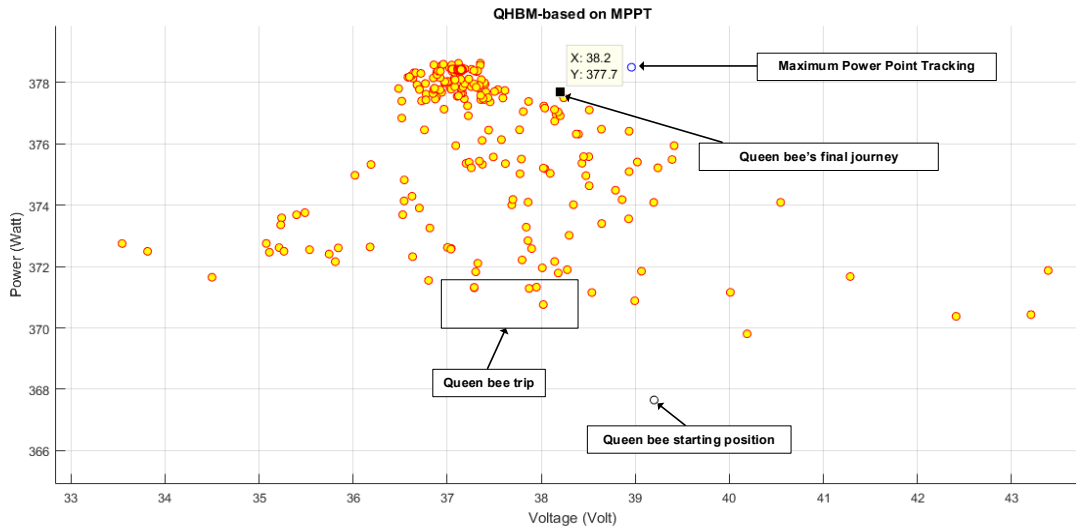**Worst QHBM-Based MPPT Simulation Results

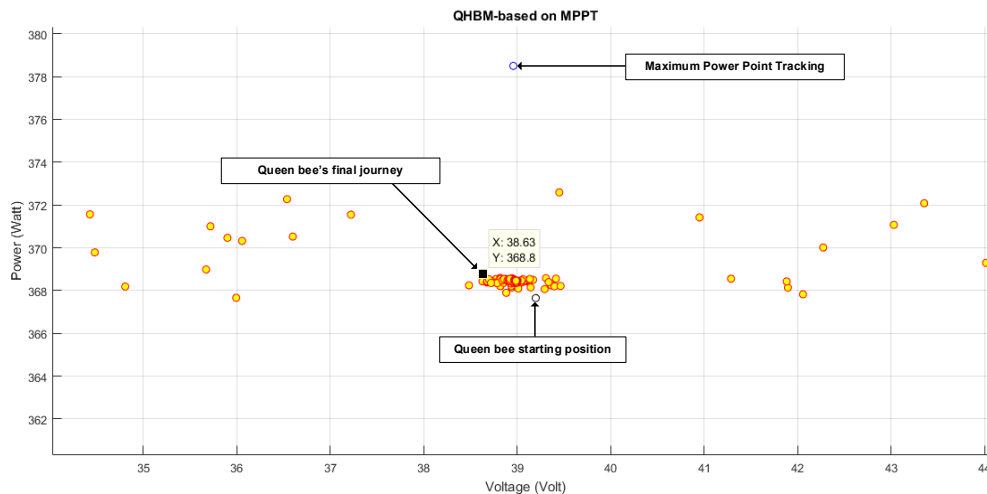Figure 14. The Best QHBM-Based MPPT Simulation

Figure 15. Worst QHBM-Based MPPT Simulation

The QHBM-based MPPT method has demonstrated commendable performance in light of the results. The optimal outcomes from the initial experiment materialized when utilizing 18 bee soldiers, a radius of 5, and a maximum iteration count of 100. In the simulation, the queen bee iterated to attain a voltage peak of 38.2 Volts, coupled with an achieved power of 377.7 Watts, vividly illustrated in Figure 14. On the flip side, the most challenging scenario emerged during the fifth experiment, involving 24 bee soldiers, a radius of 5, and a maximum iteration of 50. Within this simulation, the queen bee's iterations led to a voltage peak of 38.6 Volts, accompanied by an achieved power of 368.8 Watts, as evident in Figure 15.

Figure 14 illustrates the paramount journey towards the reference point. Within the image, a black dot marks the queen bee's inception point (Queen Bee's Initial Position). The progression of the queen bee's journey is traced by the yellow dots, each mapping her route. These waypoints are derived from the optimal probability value within that specific iteration. Subsequently, a blue dot highlights the queen bee's ultimate destination (Maximum Power Point Tracking), while a black box encapsulates the culmination of the queen bee's travel (The Bee's Last Journey).

RESULT AND ANALYSIS

Figure 16 unveils the PV power output wave, subject to QHBM computation and comparison algorithms, with a resistive load. The illustration distinctly highlights a disparity: the initial dominance of the P&O algorithm during the peak search, though this supremacy is short-lived—spanning merely from 0.5s to 2.5s—culminating in a peak of 238.4

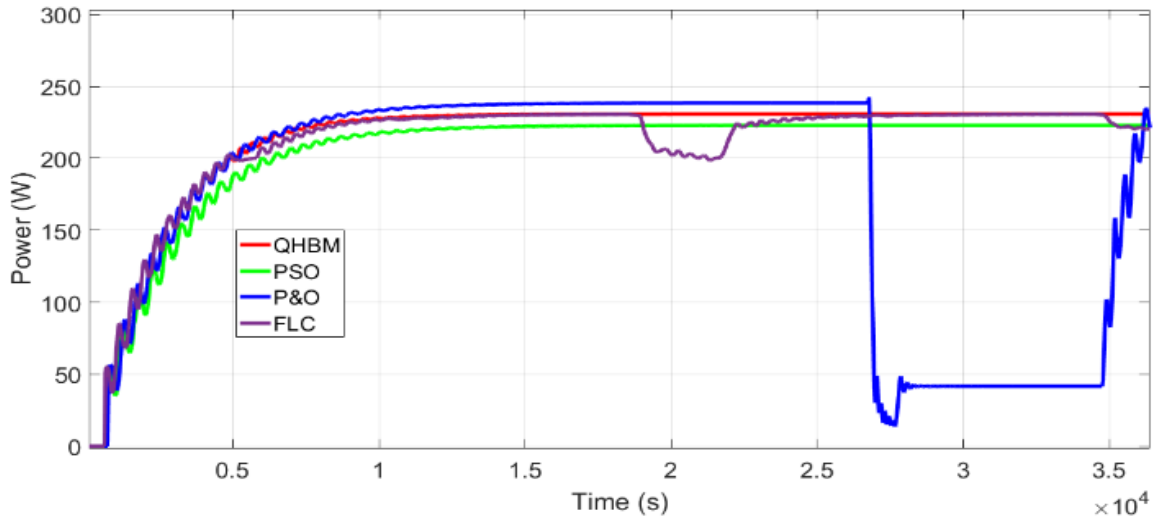Watts. A subsequent shift in the wave dynamics unfolds from 2.5s to 3.5s, yielding a peak of 41.64 Watts.

Figure 16. Tracking Time and Power Simulation Result

The wave's behavior outlines QHBM's superiority over PSO and FLC. QHBM attains a peak of 230.7 Watts over the period from 0.5s to 3.5s, surpassing P&O's achievement within the 2.5s to 3.5s timeframe. Similarly, the FLC wave reaches its pinnacle from 0.5s to 2s, netting a peak of 230.6 Watts, followed by a subsequent shift at 2s yielding a peak of 202.1 Watts. Meanwhile, PSO secures a peak of 222.7 Watts within the 0.5s to 3.5s interval. The outcomes of this resistive load comparison, encompassing tracking time and power, are systematically outlined in Table 4.

TABLE 4

COMPARISON OF TRACKING TIME AND POWER

| Radiation (W/m2)	QHBM		PSO		P&O		FLC	
	Power (Watt)	Time (Second)	Power (Watt)	Time (Second)	Power (Watt)	Time (Second)	Power (Watt)	Time (Second)
762.8	230	0.389	222	0.389	238	0.433	230	0.858
926.1	327	1.254	320	1.312	327	1.342	327	1.767
762.7	230	2.339	222	2.383	230	2.85	229	2.96
316.3	41	3.292	39.5	3.306	40	3.83	40	3.89
1053.2	376	4.186	378	4.260	376	4.74	376	4.86
304.7	38	5.301	36.7	5.389	38	5.40	37	5.88
208.3	18	6.195	17.4	6.224	36	6.69	17	6.78
935.7	332	7.324	325	7.397	332	7.353	332	7.88
158.8	10	8.292	10	8.262	10	8.84	10	8.87
257.5	27	9.172	26	9.260	37	9.201	27	9.83
240	23	10.183	23	10.213	23	10.169	23	10.9
116	5	11.21	5	11.25	6	11.09	5	11.78
170.3	12	12.16	11	12.22	12	12.61	11	12.76
233.2	22	13.18	21	13.21	22	13.71	22	13.82
182.3	14	14.20	13	14.17	13	14.78	13	14.20
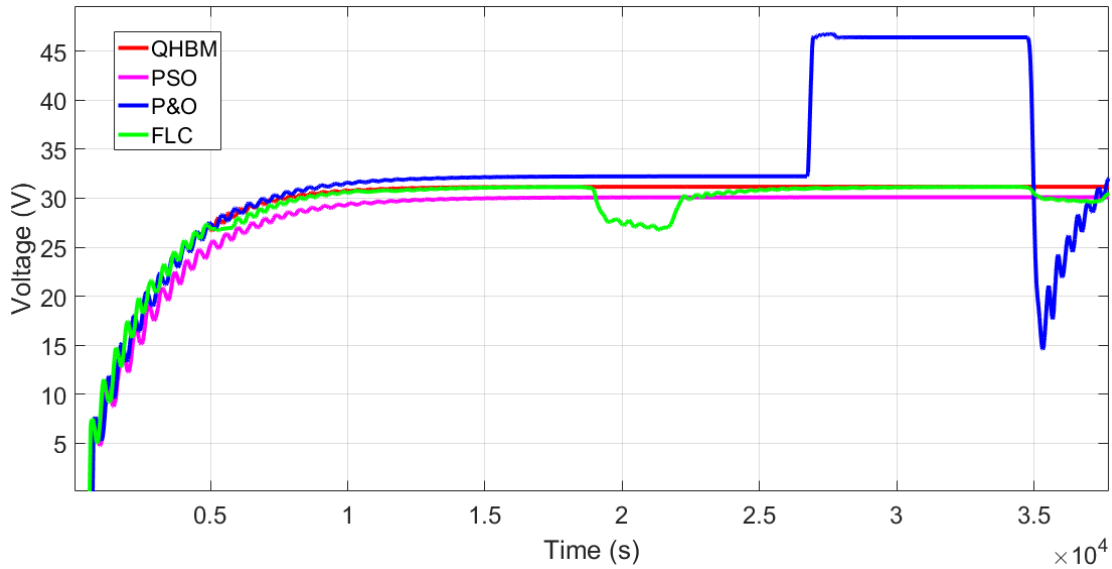
Figure 17. PV output Voltage Simulation Result

Figure 17 portrays the PV voltage output waveform, interfacing with a resistive load, as subjected to QHBM computation and comparison algorithms. Within this visualization, a discernible distinction becomes evident. During the quest for the peak voltage point, the initial P&O condition momentarily excels, seizing prominence from the outset, but this ascendancy is evanescent—lasting a mere 0.5s to 2.5s, peaking at 32.23 Volts. A subsequent alteration unfolds from 2.5s to 3s, yielding a voltage of 46.41 Volts, and a further transition emerges from 3s to 3.5s, reflecting a value of 14.65 Volts.

In stark contrast, QHBM exhibits superior performance when juxtaposed with PSO and FLC. QHBM attains a voltage peak of 31.16 Volts spanning from 0.5s to 3.5s, a feat that outshines P&O, characterized by voltage fluctuations in the 2.5s to 3.5s window, culminating in a peak of 14.65 Volts. Similarly, the FLC waveform achieves a peak voltage of 31.15 Volts within the 0.5s to 2s period, transitioning to a peak of 27.8 Volts from 2s to 2.5s. Meanwhile, PSO secures a peak voltage of 30.06 Volts over the 0.5s to 3.5s duration. The comprehensive breakdown of PV output voltage comparisons, set against a resistive load, is methodically detailed in Table 5.

TABLE 5

PV OUTPUT VOLTAGE COMPARISON

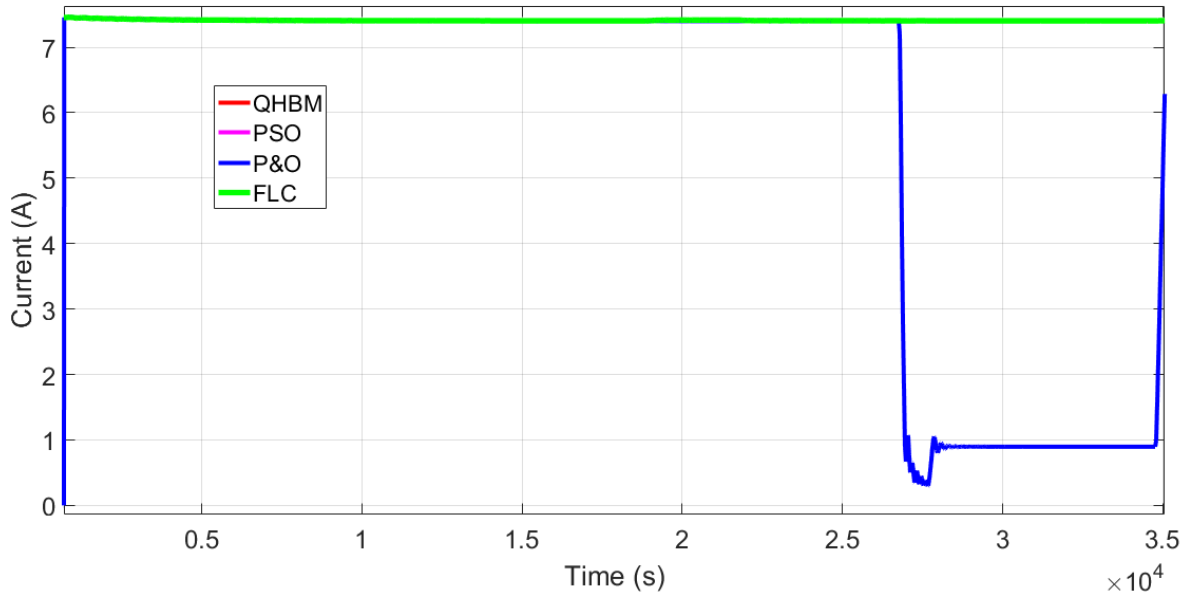| Radiation (W/m2)	QHBM	PSO	P&O
	Voltage (Volt)	Voltage (Volt)	Voltage (Volt)
762.8	31.17	30.09	32.23
926.1	37.07	36.04	37.07
762.7	31.16	30.09	31.11
316.3	13.26	12.80	13.24
1053.2	39.76	39.14	39.76
304.7	12.79	12.35	12.80
208.3	8.89	8.59	8.9
935.7	37.34	36.34	37.34
158.8	6.89	6.65	6.89
257.5	10.88	10.51	10.88
240	10.18	9.82	10.18
116	5.15	4.98	5.15
170.3	7.35	7.10	7.36
233.2	9.90	9.55	9.90
182.3	7.83	7.58	7.84

Figure 18. PV output Current Simulation Result

Figure 18 lays out the PV current output waveform interfacing with a resistive load, where QHBM computation and comparison algorithms come into play. The graphical representation brings to light a significant observation: the current output wave remains relatively stable. Across the time span from 0.5s to 3.5s, all three algorithms—QHBM, PSO, and FLC—maintain a consistent peak current value of 7.4 Amperes. In contrast, the P&O algorithm, during its prime from 0.5s to 2.5s, also achieves a peak current of 7.4 Amperes, but a transition occurs from 2.5s to 3.5s, inducing a shift in the peak current to 0.89 Amperes.

As observed in the waveform, the robustness of QHBM, PSO, and FLC algorithms remains evident throughout this time frame, sustaining the 7.4 Amperes peak current. This is contrasted with P&O's behavior, exemplifying the algorithm's responsiveness to changes in the environment. For a comprehensive breakdown of PV output current comparisons involving a resistive load, please refer to Table 6.

TABLE 6

PV OUTPUT CURRENT COMPARISON

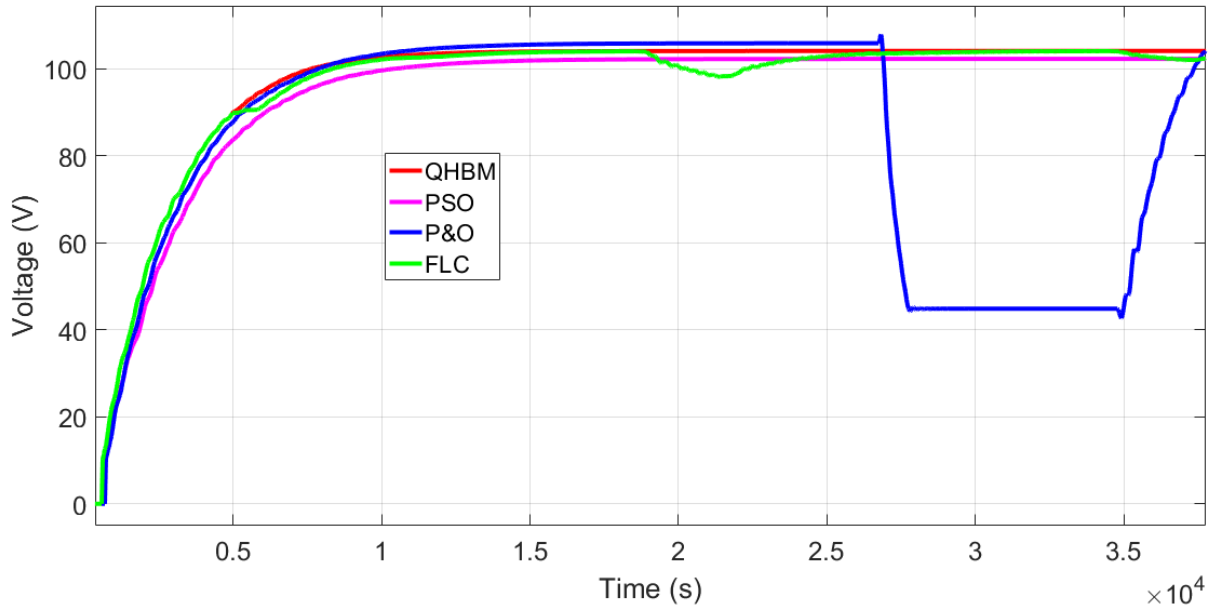| Radiation (W/m2)	QHBM	PSO	P&O	FLC
	Current (Ampere)	Current (Ampere)	Current (Ampere)	Current (Ampere)
762.8	7.4	7.4	7.3	7.4
926.1	8.8	8.8	8.8	8.8
762.7	7.4	7.4	7.4	7.4
316.3	3	3	3	3
1053.2	9.4	9.6	9.4	9.4
304.7	2.9	2.9	2.9	2.9
208.3	2	2	2	2
935.7	8.8	8.9	8.8	8.8
158.8	1.5	1.5	1.5	1.5
257.5	2.5	2.5	2.5	2.5
240	2.3	2.3	2.3	2.3
116	1.1	1.1	1.1	1.1
170.3	1.6	1.6	1.6	1.6
233.2	2.2	2.2	2.2	2.2
182.3	1.7	1.7	1.7	1.7

Figure 19. ESLLC output Voltage Simulation Result

Figure 19 elucidates the output waveform of the ESLLC, operating with a resistive load and employing QHBM computation alongside a comparison algorithm. A discernible contrast emerges from the visual representation: the QHBM waveform consistently outpaces PSO and FLC. Notably, QHBM attains a peak voltage of 104 Volts, a triumph witnessed over the time span from 0.5s to 3.5s. Within this, a notable feat is QHBM's outperformance against PSO from 2.5s to 3s in terms of peak voltage. Conversely, P&O attains a peak voltage of 44.83 Volts. Interestingly, the initial P&O condition exhibits supremacy in the quest for the peak point, maintaining the voltage within the 0.5s to 2.5s interval, achieving a peak of 105 Volts.

Furthermore, the FLC waveform attains a peak voltage of 104 Volts spanning from 0.5s to 1.5s. Subsequently, in the time span of 2s to 2.5s, FLC undergoes a transformation, resulting in a peak voltage of 98.14 Volts. Meanwhile, PSO secures a peak voltage value of 101 Volts within the 0.5s to 3.5s duration. A comprehensive breakdown of ESLLC output comparisons under a resistive load is meticulously detailed in Table 7.

TABLE 7

ESLLC OUTPUT VOLTAGE COMPARISON

Radiation (W/m2)	QHBM Voltage (Volt)	PSO Voltage (Volt)	P&O Voltage (Volt)	FLC Voltage (Volt)
762.8	104	102	105	104
926.1	124	122	124	123
762.7	104	102	104	103
316.3	43.3	42.59	43.3	43.28
1053.2	133	133	133	133
304.7	41.78	41.03	41.80	41.70
208.3	28.58	28.06	28.65	28.53
935.7	125	123	125	124
158.8	21.80	21.40	21.80	21.62
257.5	35.32	34.68	35.33	35.26
240	32.93	32.33	32.93	32.84
116	15.92	15.63	15.93	15.79
170.3	23.37	22.95	23.39	23.33
233.2	31.99	31.41	32.01	31.91
182.3	25.01	24.55	25.02	24.80

CONCLUSION

Drawing insights from the simulation results and an in-depth analysis of the QHBM-Based Maximum Power Point Tracking system, the following conclusions emerge: The QHBM Algorithm underwent parameter testing, encompassing eight distinct configurations. The optimal parameters were identified as employing 18 Scoutbees, a

radius of 5, and 100 iterations, yielding Vqueen at 38.2 Volts and Pqueen at 377.7 Watts. On the contrary, the least optimal parameters employed 24 Scoutbees, a radius of 5, and 50 iterations, yielding Vqueen at 38.6 Volts and Pqueen at 368.8 Watts. Evident from the results, the QHBM algorithm surpasses previous algorithms in terms of both speed and precision. It exhibits heightened stability over prolonged periods, distinctly outperforming the Comparison algorithm. Under resistive load conditions, the P&O Algorithm attains supremacy at an irradiation level of 762.8 W/m2, accomplishing peak point localization only within the 0.5s to 2.5s interval, registering a peak of 238.4 Watts. Beyond that, it declines from 2.5s to 3.5s, reaching a value of 41.64 Watts. In stark contrast, the QHBM algorithm outperforms PSO and FLC, attaining a peak of 230.7 Watts within the 0.5s to 3.5s timeframe, surpassing P&O, which exhibits changes within the 2.5s to 3.5s interval. The FLC algorithm secures a peak from 0.5s to 2s, peaking at 230.6 Watts, followed by a shift at 2s, reaching 202.1 Watts. Meanwhile, the PSO algorithm achieves a peak of 222.7 Watts within the time frame of 0.5s to 3.5s.

The QHBM algorithm boasts faster computation and prolonged stability, albeit with an initial challenge of finding the starting point for MPP tracking due to random parameter retrieval. The PSO algorithm excels in swiftly adapting to environmental changes, although it suffers from lengthy computational time. The commercial usability of the P&O algorithm is offset by convergence and oscillation problems in MPP tracking, often failing to manage environmental shifts. Lastly, the FLC algorithm adeptly handles rapid environmental changes but demands computational complexity. In essence, the QHBM-Based MPPT system exhibits superior performance, blending rapid computation with stability. This comprehensive understanding underscores its potential for enhancing solar power system efficiency and effectiveness.

ACKNOWLEDGMENT

REFERENCES

[1] F. Blaabjerg, M. Lonel., Renewable Energy Devices and System with Simulations in Matlab and ANSYS. Renewable Energy Sources, pp. 978-4987, 2016, https://Blaabjerg lonel/p/book/9780367656218.

[2] L. M. Elobaid, A. K. Abdelsalam and E. E. Zakzouk, "Artificial neural network-based photovoltaic maximum power point tracking techniques a survey," in *IET Renewable Power Generation*, pp. 1043-1063, 2015, https://doi.org/10.1049/iet-rpg.2014.0359.

[3] M. A. Green, Y. Hishikawa, E. D. Dunlop. D. H. Levi. J. Hohlebinger, and A. W. Y. Ho-Baillie, "Solar cell efficiency tables," *Progress in Photovoltaic Research and Applications*, pp. 3-12, 2018, https://doi.org/10.1002/pip.2978.

[4] J. M. Enrique, J. M. Andujar, M. A. Bohorquez, "A reliable, fast and low cost maximum power point tracker for photovoltaic applications," in *Solar Energy*, pp. 79-89, 2010, https://science/article/abs/pii/S0038092X09002527.

[5] E. Kandemir, N. S. Cetin and S. Borekci, "An Investigation of Intelligent and Conventional Maximum Power Point Tracking Techniques for Uniform Atmospheric Conditions," in *ENJES Europen Journal of Engginering and Natural Sciences*, pp. 93-100, 2019, https://dergipark.org.tr/en/pub/ejens/issue/49410/370811.

[6] K. Sundareswaran, V. Vignesh kumar, and S. Palani, "Application of a combined particle swarm optimization and perturb and observe method for MPPT in PV systems under partial shading conditions," *Renewable Energy*, pp. 308-317, 2015, https://science/article/abs/pii/S0960148114006090.

[7] B. Bendip, H. Belmili, and F. Krim, "A survey of the most used MPPT methods: Conventional and advanced algorithms applied for photovoltaic systems," *Renewable and Sustainable Energy Reviews*, pp. 637-648, 2015, https://academia.edu/28589183.

[8] H. Islam, S. Mekhilef. N. B. M. Shah, T. K. Soon, M. Seyedmahmousian, B. Horan and A. Stojcevski, "Performance Evaluation of Maximum Power Point Tracking Approachhes and Photovoltaic System. in *ENERGIES*, pp. 33-90, 2018, https://www.mdpi.com/1996-1073/11/2/365.

[9] S. N. Kamat and R. Shenbagalakshmi, "Design and Analysis of Positive Output Self Lift Luo Converter," *Fourth International Conference on Computing Communication Control and Automation (ICCUBEA)*, pp. 1-6, 2018, https://doi.org.10.1109/pip.8697578.

[10] S. Amirtharja and L. Premalatha, "Design of an Efficient Positive Output Self-Lift and Negative Output Self-Lift Luo Converers using Drift Free Technique for Photovoltaic Applications," *Internatonal Conference on Power Engineering, Computing and Control*, pp. 651-657, 2017, https://science/article/pii/S1876610217323937.

[11] G.-J. Jong, Aripriharta, Hendrick, and G.-J. Horng. 2017. A Novel Queen Honey Bee Migration (QHBM) Algorithm for Sink Repositioning in Wireless Sensor Network. Wireless Personal Communications. 3209–3232. https://springerprofessional/12036788.

[12] International Renewable Energy Agency https://irena.org.

[13] N. Femia, G. Petrone, G. Spagnuolo and M. Vitelli. 2012. Power Electronics and Control Techniques for Maximum Energy Harvesting in Photovoltaic System. Industrial Electronics. 366-365. https://Femia/p/book/9781466506909.

[14] Wibowo. K. H, Aripriharta, Fadlika. I, Horng. G. J, Wibawanto. S, and Saputra. F. W. Y. 2019. A New MPPT based on Queen Honey Bee Migration (QHBM) in Standalone Photovoltaic. International Conference on Automatic Control and Intelligent System.123-128. https://ieeexplore.ieee.org/document/8825025.

[15] S. Amirtharja and L. Premalatha.2017. Design of an Efficient Positive Output Self-Lift and Negative Output Self-Lift Luo Converers using Drift Free Technique for Photovoltaic Applications. Internatonal Conference on Power Engineering, Computing and Control. 651-657. https://doi.org 10.1016/j.egypro.2017.05.167.

[16] F. L. Luo and H. Ye. 2003. Advance DC/DC Converters. Engineering and Technology. 1-792. https://doi.org/10.1201/9780203492925.

[17] Datasheet NSP D6M360E. https://mitsubishielectricsolar.